Simulation of Field-induced Chiral Phenomena in Inhomogeneous Superconductivity

Hirono Kaneyasu, Kouki Otsuka, Singo Haruna, Shinji Yoshida and Susumu Date

Abstract We explain the field-induced chiral phenomena in inhomogeneous superconductivity and perform a computational simulation to demonstrate such phenomena on the basis of the Ginzburg–Landau equation for the inhomogeneous interface superconductivity of a eutectic system. Field-induced chiral phenomena occur because of the paramagnetic coupling of an intrinsic magnetization with an external magnetic field. Applying a magnetic field to a non-chiral state leads to a field-induced chiral transition with the generation of a paramagnetic chiral current. Numerically solving the aforementioned equation yields converged solutions and output numerical data obtained through an iterative process. The actual time for this calculation can be distinctly reduced through acceleration via code optimization that is suitable for vector parallelization. Reducing the calculation time makes it possible to extend the simulation to lower temperatures where the inhomogeneous superconductivity spreads to a greater distance from the interface.

Hirono Kaneyasu, Kouki Otsuka and Shingo Haruna
Graduate School of Science, University of Hyogo, Japan, e-mail: hirono@sci.u-hyogo.ac.jp

Shinji Yoshida
Graduate School of Information Science and Technology, Osaka University, Japan

Susumu Date
Cybermedia Center, Osaka University, Osaka, Japan

1 Field-induced chiral phenomena in inhomogeneous superconductivity

1.1 Chiral state

Superconductivity is a valuable feature of energy and electric technologies. Electric properties and electromagnetic features are used in power transmission, magnetic, and quantum devices. The superconducting state appears when the temperature is lowered and two electrons form a pair known as the Cooper pair. Electromagnetic features can be understood from the microscopic aspect of electron pairs [1, 25]. The electron pairs condense in the same quantum state, leading to the macroscopic phenomenon of superconductivity.

The features of a Cooper pair are characterized by the "spin" and "orbital" of the electrons in the quantum state, as shown in Fig. 1 (a). The spin configuration is anti-parallel or parallel, referred to as spin-singlet and spin-triplet states, respectively. Meanwhile, the intrinsic angular momentum L_z for an orbital of a Cooper pair is characterized by an intrinsic magnetization denoted by $L_z \neq 0$, i.e., $L_z = \pm 1, \pm 2, ...$, which reflects a chiral state with the time-reversal symmetry breaking [17, 32]. The superconducting state with intrinsic magnetization causes interesting chiral phenomena that differ from usual superconductivity.

1.2 Field-induced chiral phenomena

In the chiral state, an electron pair with intrinsic magnetization has a feature response to an external magnetic field because the intrinsic magnetization couples with the external magnetic field [23]. A part of this is the field-induced chiral phenomena, which results from the paramagnetic coupling of the intrinsic magnetization with an external magnetic field [9, 23]. The paramagnetic coupling of the intrinsic magnetization stabilizes the chiral state by generating a paramagnetic chiral current in the direction opposite to the screening current, as shown in Fig. 1 (b) [9, 23]. By contrast, the screening current flows to generate a diamagnetic field to the external magnetic field. This is known as the Meissner effect, which is a general feature of superconductivity [24]. Such field-induced chiral phenomena occur distinctly in the case of inhomogeneous superconductivity, which has been reported in a theoretical study based on the Ginzburg–Landau theory [9].

In inhomogeneous superconductivity, the application of a magnetic field to a non-chiral state causes the field-induced chiral transition with the generation of a paramagnetic chiral current, as shown in Fig. 2 (a) [9]. For example, such a non-chiral state yields an onset temperature of superconductivity as an interface state nucleating near the interface between superconductivity and a metal, which transits to a chiral state when the temperature is lowered in a zero field [9, 11, 12, 31]. Such an interface system is a characteristic of a eutectic superconductor containing multiple

interfaces between the parent superconductor and metal inclusions. Identifying the field-induced chiral phenomena in such materials is useful for discovering candidates for chiral superconductors, because the field-induced chiral phenomena constitute evidence of chiral superconductivity.

In this study, a computational simulation is conducted to demonstrate the field-induced chiral phenomena with a paramagnetic chiral current in the inhomogeneous state. In particular, the field-induced chiral transition is produced in an interface superconducting model for eutectic Sr_2RuO_4-Ru [19–21]. The features of the field-induced chiral phenomena are qualitatively compared with the experimental results obtained for eutectic Sr_2RuO_4-Ru [14, 20, 36]. The good agreement with the experimental results serves as evidence of a chiral state in the bulk state of the parent superconductor Sr_2RuO_4 [9].

2 Field-induced chiral phenomena in a eutectic superconductor

2.1 Inhomogeneous interface superconductivity

Sr_2RuO_4 is a potential candidate for chiral superconductors [6, 18, 35]. The parent material of eutectic Sr_2RuO_4-Ru is Sr_2RuO_4, which contains micrometer-scale Ru-metal inclusions [20, 21]. Experiments have reported the nucleation of inhomogeneous superconductivity around interfaces between the Ru-metal inclusions and the parent superconductor Sr_2RuO_4. Inhomogeneous interface superconductivity exhibits an intrinsic magnetization below the bulk transition temperature $T_{\rm bulk}$ near $T_{\rm c,SRO} = 1.5$ K, which is the superconducting transition temperature of pure Sr_2RuO_4 [30]. Moreover, theoretical studies have suggested that the superconducting phenomena are evidence of a chiral state in the parent superconductor Sr_2RuO_4 [3, 9, 11–13, 22, 31].

In the eutectic superconductor Sr_2RuO_4-Ru, the inhomogeneous interface state asymptotes to a superconducting state of pure Sr_2RuO_4 when the temperature is lowered to $T_{\rm c,SRO}$. By contrast, interface superconductivity appears at the onset temperature $T_{\rm onset}$, i.e., 3 K above $T_{\rm bulk}$. When the temperature is lowered in a zero field, first, the interface state is a non-chiral state near $T_{\rm onset}$; thereafter, the non-chiral state transits to a chiral state when T is lowered toward $T_{\rm bulk}$. This interface superconducting model for explaining the chiral transition is considered for the 3-Kelvin phase model of eutectic Sr_2RuO_4-Ru [31]. The interface superconductivity nucleates in accordance with the increase in the superconducting transition temperature locally near the interface originating from a particular electron state induced by strain due to the deposition of Ru-metal inclusions [7, 33, 37]. This interface model is shown in Fig. 2 (b) [9, 11, 12, 31]. Considering a Ru-metal inclusion in the parent superconductor Sr_2RuO_4, a planar interface perpendicular to a RuO_2-layer is set at the junction Ru/Sr_2RuO_4.

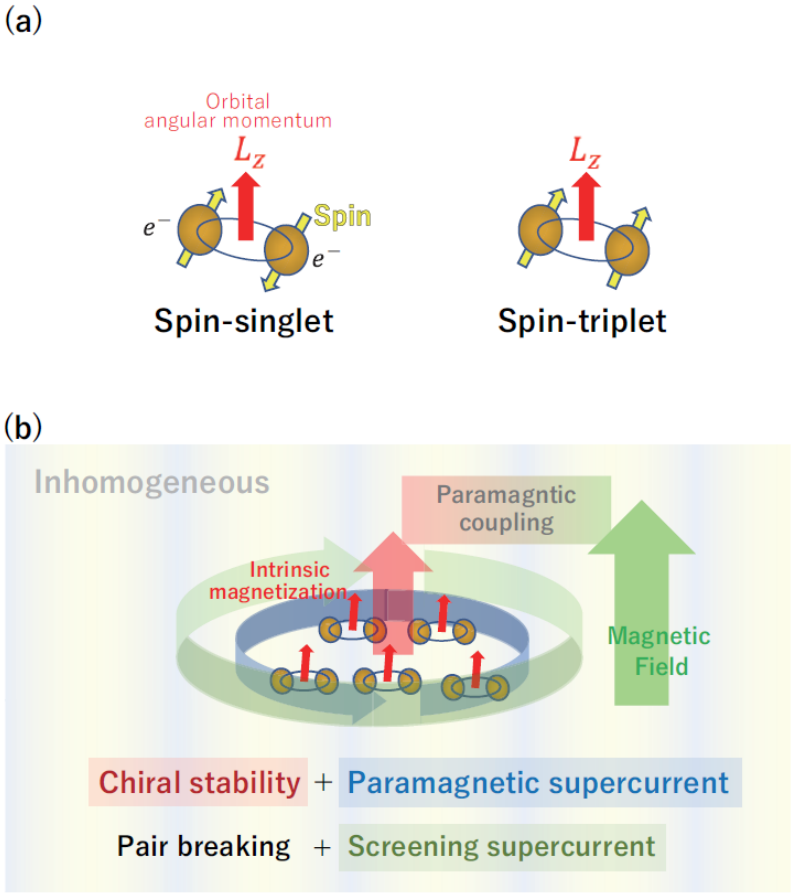

Fig. 1: (a) Chiral state of the Cooper pair in configurations of spin and angular momentum. The intrinsic angular momentum for the orbital of the Cooper pair is $L_z \neq 0$, i.e., $L_z = \pm 1, \pm 2, \ldots$. (b) Field-induced chiral phenomena in inhomogeneous superconductivity. The chiral state is stabilized by applying an external magnetic field with the generation of a paramagnetic chiral supercurrent that flows in the direction opposite to the screening supercurrent, whose field is diamagnetic to the external magnetic field.

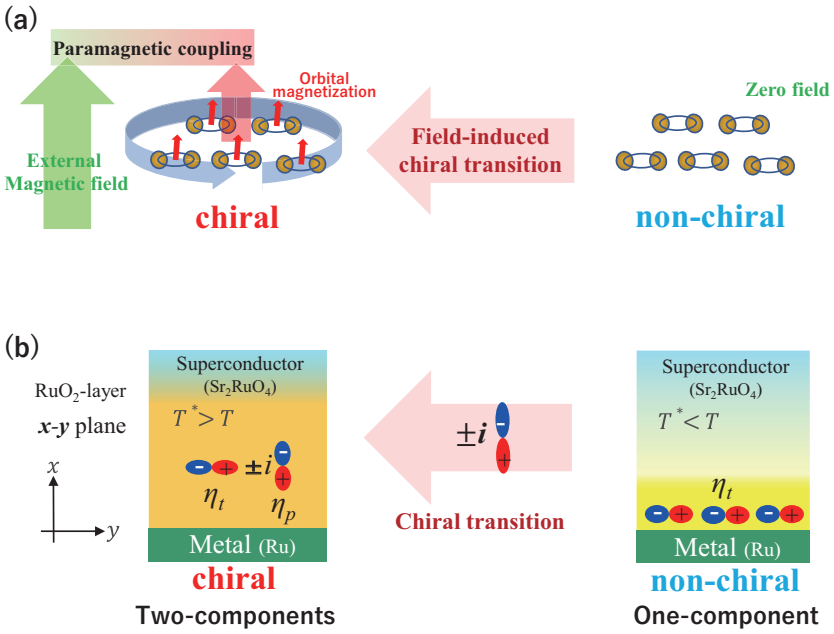

Fig. 2: (a) Field-induced chiral transition in inhomogeneous superconductivity. The chiral state stabilizes owing to the paramagnetic coupling of an intrinsic magnetization with an external magnetic field, and it generates a paramagnetic chiral supercurrent. (b) Order parameter $\boldsymbol{\eta}$ of inhomogeneous superconductivity near an interface between a metal and a superconductor, i.e., Ru/Sr_2RuO_4. The chiral state is represented by two components η_t and η_p in the xy-plane parallel to the RuO_2-layer, and this is common to the chiral states $k_{zx} \pm ik_{yz}$ and $k_x \pm ik_y$ in the projection to the xy-plane. Here, η_t and η_p denote the tangential and perpendicular components, respectively. A two-component state with both η_t and η_p and a one-component state with only η_t correspond to the chiral and non-chiral states, respectively. The chiral transition corresponds to a transition from the one-component state to the two-component state due to yielding the second component η_p [31].

2.2 Chiral transition represented with order parameter

Here, we assume that a chiral state for a bulk state below T_{bulk} is identical to that for pure Sr_2RuO_4, as shown in Fig. 2 (b). Considering a point group D_{4h} for a perovskite structure of pure Sr_2RuO_4, some of the possible chiral states are a chiral d-wave, $d_{zx} \pm id_{yz}$, and a chiral p-wave state, $p_x \pm ip_y$, protected by the symmetry of crystal structure, as well as a chiral d-wave, $d_{x^2-y^2} \pm id_{xy}$ in accidental degeneracy [5, 15]. In a traditional classification, $d_{zx} \pm id_{yz}$ and $d_{x^2-y^2} \pm id_{xy}$ are the spin-singlet state, while $p_x \pm ip_y$ is the spin-triplet state [32]. Their intrinsic magnetization is parallel

to the z-axis, corresponding to an angular momentum $L_z \neq 0$ for the Cooper pair. The crystalline structure along the z-axis is perpendicular to the RuO_2 layers on the xy-plane, leading to the two-dimensional electron property. Projecting onto the xy-plane of the RuO_2-layer, the components of the order parameter on the xy-plane are common to both chiral states with $d_{zx} \pm id_{yz}$ and $p_x \pm ip_y$ represented using $k_z k_x \pm ik_y k_z$ and $k_x \pm ik_y$, respectively, as shown in Fig. 2 (b) [9, 11, 12, 22, 31].

The chiral states with the time-reversal symmetry breaking are denoted with a combination of two orbital symmetries with a pure imaginary number i, corresponding to $\eta_t + i\eta_p$ in the expression of a superconducting order parameter. Here, the components η_t and η_p of the order parameters correspond to the tangential and perpendicular components of interface Sr_2RuO_2/Ru, respectively. By contrast, a non-chiral state is represented with only one component η_t. Therefore, a chiral transition indicates a transition from the one-component state with η_t to the two-component state with $\eta_t + i\eta_p$, yielding the second component η_p [32].

This interface model sets a superconducting transition temperature that increases near the interface; moreover, it sets boundary conditions for the suppression of the perpendicular components at the interface in the extrapolates of superconductivity to the interface between the Ru-metal and the Sr_2RuO_4-superconductor [9, 11, 12, 22, 31]. The nucleation of superconductivity at the interface originates from the local enhancement of the superconducting transition temperature in a narrow range at the interface on the side of Sr_2RuO_4. In addition, the component η_p, which is perpendicular to the interface, is suppressed by the boundary conditions for the interface. In this situation, the non-chiral state is stabilized with the nucleation of only one component η_t in a zero field at $T_{\mathrm{onset}} = 3$ K. This non-chiral state with one component η_t transits to the chiral state with two components $\eta_t + i\eta_p$ at $T^* = 2.3$ K by yielding the second component η_p, owing to the lowering of the temperature in the zero field.

As T^* is a chiral transition temperature due to the lowering of the temperature in the zero field above T^*, the non-chiral state is stabilized with one component η_t in the zero field. When a magnetic field H_z is applied to this non-chiral state with one component η_t above T^*, it transits to the chiral state with two components $\eta_t + i\eta_p$ by yielding the second component η_p as the field-induced chiral transition.

In addition to their chiral state candidates, theoretical studies have also suggested other candidates [4, 15, 26, 28, 29, 34].

2.3 Simulation of field-induced chiral transition

Assuming the chiral states $d_{zx} \pm id_{yz}$ and $p_x \pm ip_y$ as a bulk phase in the eutectic Sr_2RuO_4-Ru, the simulation demonstrates the field-induced chiral phenomena in the inhomogeneous interface phase by applying a z-axis magnetic field H_z parallel to an intrinsic magnetization of the chiral Cooper pair, as shown in Figs. 3, 4, and 5. By numerically solving the Ginzburg–Landau equation, which is set using parameters common to $k_z k_x \pm ik_y k_z$ and $k_x \pm ik_y$ for $d_{zx} \pm id_{yz}$ and $p_x \pm ip_y$, respectively,

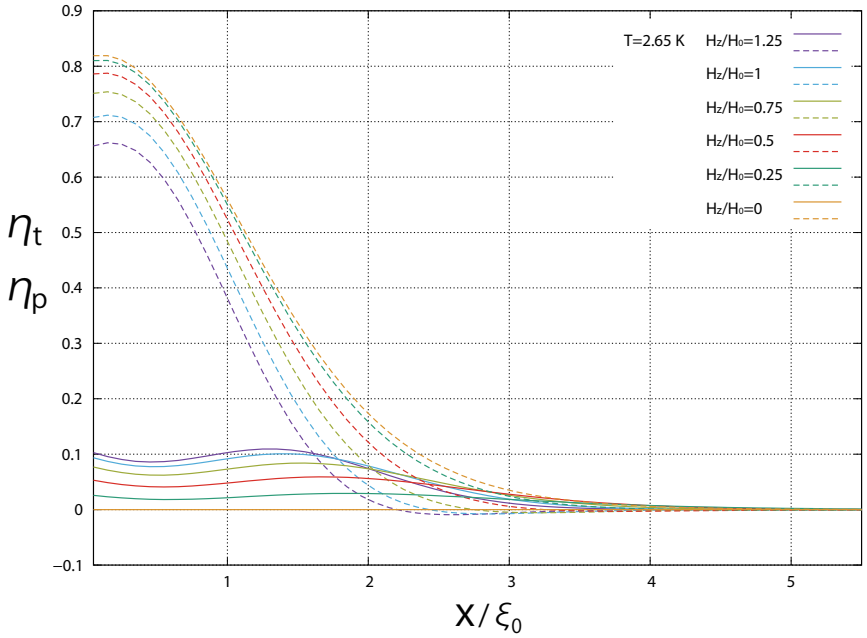

Fig. 3: Two components η_t and η_p of the order parameter dependent on x at T = 2.65 K. The perpendicular component η_p is plotted with solid lines, whereas the tangential component η_t is plotted with dashed lines. An external magnetic field H_z parallel to the z-axis varies in units of H_0, where H_0 is the critical field and ξ_0 is the coherence length of pure Sr_2RuO_4 at $T = 0$. The magnetic field H_z is given in units of H_0 = 0.075 T, compared with the experimental critical field of Sr_2RuO_4-Ru [9, 36]. The non-chiral state is stabilized with the nucleation of only one component η_t in a zero field at T = 2.65 K, as this temperature is above the chiral transition temperature T^* = 2.3 K due to lowering temperature in a zero field. The non-chiral state, i.e., the state with one component η_t, transits to the chiral state, i.e., the state with two components $\eta_t + i\eta_p$, by yielding the second component η_p under the application of the magnetic field H_z, indicating a field-induced chiral transition.

the two components, η_p and η_t, of the superconducting order parameters and the vector potential $\boldsymbol{A}$ are obtained as numerical solutions [9, 11, 12, 22, 31]. The chiral transition is shown with η_p and η_t in Fig. 3, and 4, and paramagnetic and screening supercurrents are calculated from η_p, η_t, and $\boldsymbol{A}$ [9], as shown in Fig. 5.

An interface model sets the critical superconducting temperature enhancing near the interface, as well as the boundary conditions such that a perpendicular component η_p is suppressed at the interface [9, 11, 12, 22, 31]. According to this setting, η_t and η_p depend on the position x from the interface, as shown in Fig.2 (b); thus a superconducting order parameter and a vector potential $\boldsymbol{A}$ depend on the position x. As the intrinsic magnetization and the external field are parallel to the z-axis, and

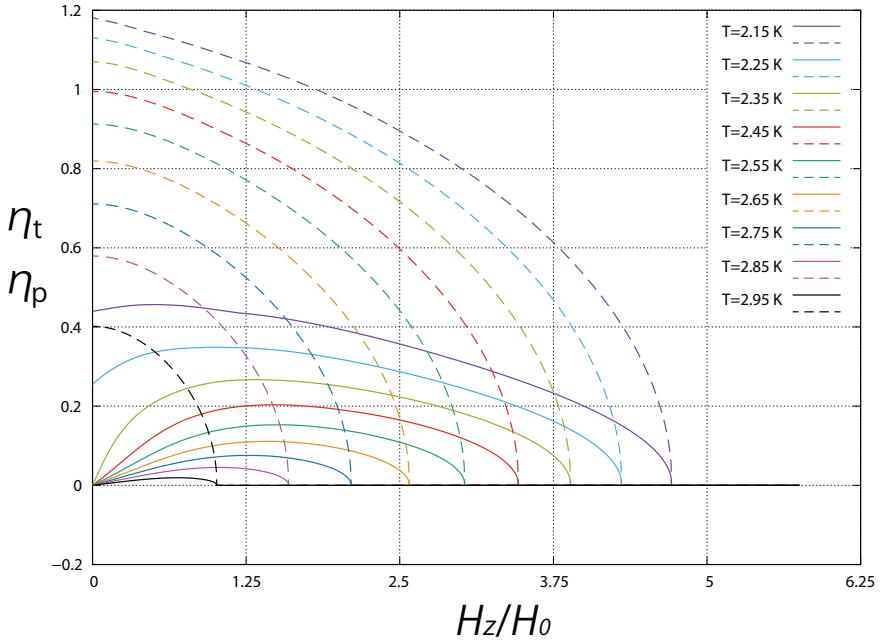

Fig. 4: Dependence of the maximum values of the two components η_t and η_p on an external magnetic field H_z. When the magnetic field is applied to the non-chiral state above $T^* = 2.3$ K, a chiral transition occurs by yielding η_p.

the $\boldsymbol{A}$ includes an intrinsic magnetic field and an external magnetic field H_z parallel to a z-axis, setting $\boldsymbol{A} = (0, A_y, 0)$ connects to a total magnetic field B_z through $\boldsymbol{B} = \boldsymbol{\nabla} \times \boldsymbol{A}$.

In this one-dimensional model, the following is the Ginzburg–Landau equation with the two components, η_t and η_p, of the order parameter for the chiral state [9, 11, 12, 22, 31]

$$
\begin{aligned}
a\eta_t + \frac{1}{4}b\eta_t(3\eta_t^2 + \eta_p^2) - K_2\partial_x^2\eta_t + \gamma^2 A_y^2 K_1\eta_t - \gamma K_{3,4}(\partial_x\eta_p A_y + A_y\partial_x\eta_p) = 0, \\
a\eta_p + \frac{1}{4}b\eta_p(3\eta_p^2 + \eta_t^2) - K_1\partial_x^2\eta_p + \gamma^2 A_y^2 K_2\eta_p + \gamma K_{3,4}(\partial_x\eta_t A_y + A_y\partial_x\eta_t) = 0,
\end{aligned}
\tag{1}
$$

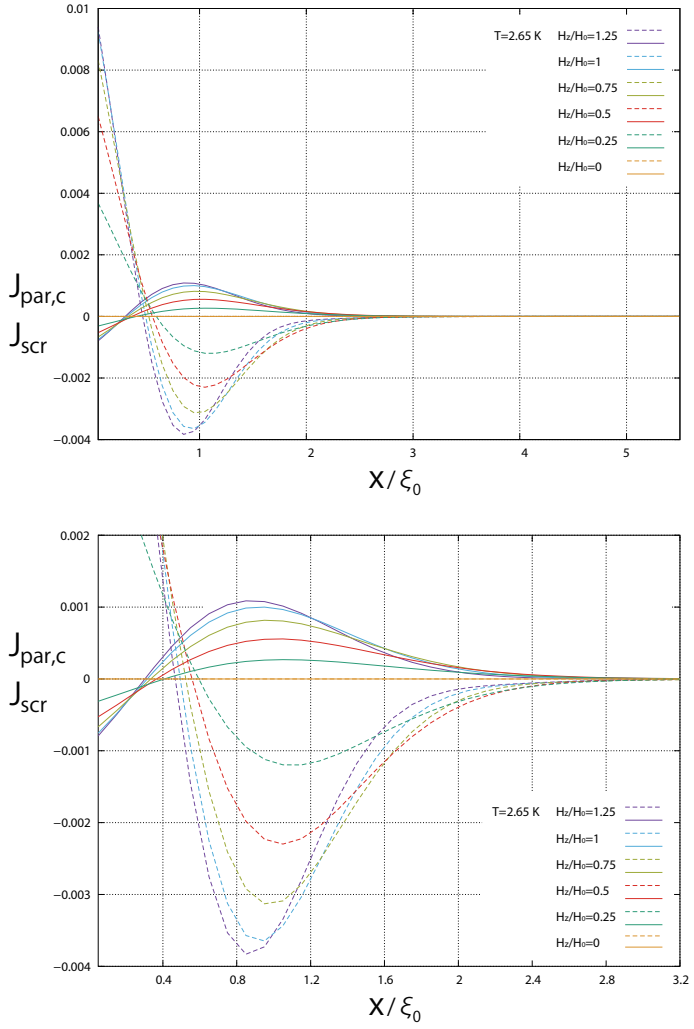

Fig. 5: Field-induced supercurrents dependent on x at T = 2.65 K. The upper panel shows the overall view, and the lower panel shows partial magnification. The paramagnetic chiral current $J_{\mathrm{par,c}}$ is plotted with solid lines, and the screening current J_{scr} is plotted with dashed lines. An external magnetic field H_z parallel to the z-axis varies in units of H_0, where H_0 is the critical field and ξ_0 is the coherence length of pure Sr_2RuO_4 at T = 0. Both currents have extremely small values, i.e., nearly zero in a zero field, and both currents are induced in a magnetic field. The paramagnetic current $J_{\mathrm{par,c}}$ increases by stabilizing a chiral state by strengthening the magnetic field visible in the order parameter, as shown in Fig. 3, while the screening current also increases by shielding the strengthening magnetic field.

where the parameters for gradient terms are set as $K_2 = K_{3,4} = K_1/3$. The coefficient a is set as $a = a(T) = a'(T - T_c(x))/T_{c,SRO}$ with $a' > 0$ and a x-dependent critical superconducting temperature $T_c(x)$ [9, 11, 12, 22, 31]. An onset of interface superconductivity at 3 K sets with $T_c(x) = T_{c,SRO} + T_0/\cosh(x/w)$ through arranging the narrow width w and the enhancement T_0 [9, 11, 12]. In contrast, the bulk phase is below the superconducting transition temperature $T_{c,SRO}$ of the pure Sr_2RuO_4.

On the other hand, the boundary conditions at the interface at $x = 0$ are set for the interface superconductivity [9] as follows

$$\begin{aligned} K_1 \partial_x \eta_p(x)\big|_{x=0} &= \frac{1}{l_p}\eta_p(0) + \gamma A_y(0) K_{3,4}\eta_t(0), \\ K_2 \partial_x \eta_t(x)|_{x=0} &= -\gamma A_y(0) K_{3,4}\eta_p(0), \end{aligned} \tag{2}$$

where l_p is an extrapolation length in which the superconductivity extrapolates to the Ru-metal through the interface; meanwhile, the perpendicular component η_p is suppressed at the interface. The formulation of the supercurrent [9] is as follows,

$$j_y(x) = 8\pi \left[-\gamma^2 A_y (K_1|\eta_p|^2 + K_2|\eta_t|^2) + \gamma K_{3,4}(\eta_t \partial_x \eta_p - \eta_p \partial_x \eta_t)\right], \tag{3}$$

where the $K_{3,4}$-term is a paramagnetic chiral current, and the K_1, K_2-term is a screening current.

Note that the Ginzburg–Landau equation, i.e., Eq. (1), for $d_{zx} \pm id_{yz}$ and $p_x \pm ip_y$, has a symmetry common to that of $d_{x^2-y^2} \pm id_{xy}$, while the parameters for $d_{zx} \pm id_{yz}$ and $p_x \pm ip_y$ differ from those of $d_{x^2-y^2} \pm id_{xy}$. This common symmetry leads to qualitatively identical field-induced chiral phenomena despite the difference in parameters.

Demonstrating the field-induced chiral transition by applying H_z, Fig. 3 shows the components of the order parameter depending on the distance x from the interface Sr_2RuO_4/Ru. The change in the two components η_t and η_p depends on the magnetic field, which leads to a field-induced chiral transition at $T = 2.65$ K. In a zero field $H = 0$, the state at $T = 2.65$ K is a non-chiral state that stabilizes near T_{onset} as the onset temperature. The non-chiral state represents only one component η_t of the order parameter, i.e., the tangential component, which is enhanced near the interface, whereas the perpendicular component η_p becomes zero by suppression through the effect of the interface. On applying a magnetic field to the non-chiral state in a zero field, the perpendicular component η_p increases from zero and appears as the second component. Subsequently, a transition to a chiral state occurs, representing both the components η_t and η_p, which is the field-induced chiral transition. Here, the components of the order parameter are enhanced near an interface because the inhomogeneous interface state is localized near a Ru-metal inclusion that originates from the enhancement of the superconducting transition temperature near a Ru-metal/Sr_2RuO_4-superconductor interface. In this model, it is assumed that a chiral state exists in the bulk state below T_{bulk}.

Fig. 4 shows the field dependence of the maximum values of the two components η_t and η_p with respect to the distance. The non-chiral state appears with only one component η_t above $T^* = 2.3$ K in a zero field $H = 0$. When an external magnetic field is applied to the non-chiral state, the second component η_p newly appears owing to the field-induced chiral transition. The value of vertical component η_p increases by the strengthening the magnetic field, indicating that the further stabilization of the chiral state. In contrast, the tangential component η_t decreases under the application of the field. Additionally, by further strengthening the field, η_t and η_p decrease, and then both are reduced to zero when the magnetic field is strengthened to the critical magnetic field H_{c2}, where the superconductivity vanishes.

The computational simulation shows the field-induced chiral transition, i.e., a non-chiral state transits to a chiral state under the application of a magnetic field parallel to an intrinsic magnetization in a model that assumes that the bulk phase is in a chiral state. An existing study has reported field-induced chiral stability with the *H-T* phase diagram in detail [9], which qualitatively consists of the field dependence of a zero-bias anomaly in a differential conductance of quasi-particles, observed via tunneling spectroscopy for the interface of Ru/Sr_2RuO_4 [14,36]. There is a qualitative agreement between the theoretical and experimental results under the assumption that the bulk state is in a chiral state; this is evidence that a pure Sr_2RuO_4 has a chiral state [9].

2.4 Paramagnetic chiral supercurrent

Next, we show the paramagnetic chiral supercurrent in Sr_2RuO_4-Ru in Fig. 5. The field-induced chiral stability causes paramagnetic supercurrents. Moreover, the inversion of chirality occurs at a certain distance. The total supercurrent comprises both the paramagnetic chiral current and the screening current. The paramagnetic current can be attributed to the paramagnetic coupling with an external magnetic field. By contrast, the screening current persists because the superconductivity ejects the external magnetic field [9, 11].

3 Computation of field-induced chiral phenomena

The Ginzburg–Landau equation in Eq. (1) is a variational equation derived from the Ginzburg–Landau free energy. It is a simultaneous differential equation with boundary conditions at the interface. The numerical calculation for solving the equation involves the use of the quasi-Newton method. The flowchart of the calculation process for the algorithm is shown in Fig. 6 (a). As solutions of the simultaneous equation, we obtain two components η_t and η_p of the order parameter and a vector potential A_y, which corresponds to H_z through $\boldsymbol{B} = \boldsymbol{\nabla} \times \boldsymbol{A}$. Consistent solutions are obtained when the iterative calculation process converges, as shown in Fig. 6

(b). The supercurrent is calculated using three solutions: η_t, η_p, and A_y; a paramagnetic chiral current $J_{\mathrm{par,c}}$ and a screening current J_{scr} are thus obtained. Meanwhile, the two components η_t and η_p are expressed as changes in the order parameter responsible for the field-induced chiral transition. In addition, the dependence of the order parameter on the distance from the interface indicates an inversion of the intrinsic magnetization as a change in the sign of one component, i.e., η_t [10]. The field-induced chiral transition, paramagnetic chiral current, and inversion of intrinsic magnetization with the distance originate from the paramagnetic coupling of an intrinsic magnetization with an external magnetic field, and the three field-induced phenomena are related by a calculation based on the convergent solutions of the Ginzburg–Landau equation, as shown in Fig. 6 (b).

The long calculation time required for obtaining solutions to the quasi-Newton method depends on the size of the calculation, which varies with the temperature and magnetic field, as well as the mesh number used to divide the distance. We performed this calculation using SX-ACE and the SX-Aurora TSUBASA at the Cybermedia Center, Osaka University, and Cyberscience Center, Tohoku University [2, 16]. The iteration for mesh numbers greater than 240 is performed using vectorization with a vector engine. A long time is required for the numerical calculation when the temperature and magnetic field are sufficiently varied for evaluating the field-induced chiral stability in inhomogeneous superconductivity. Moreover, the required calculation time increases by considering a greater distance to evaluate the dependence of the order parameter on the distance from the interface. In order to reduce this calculation time, code-tuning improves the vectorization rate from 94.4% to 99.4%, significantly reducing the calculation time by 68% [38].

Acceleration via code-tuning makes it possible to analyze the field-induced chiral phenomena in a shorter calculation time. To study the field dependence of the chiral state near the bulk phase, a long distance must be set in the calculation because the order parameter further away from the interface when the temperature is lowered toward T_{bulk}. Moreover, to evaluate the gradient terms of the equation in detail, the mesh number must be increased because the order parameter and vector potential vary depending on the distance. This requires a longer calculation time. Reducing the calculation time is an effective method to increase the distance, and it is possible to extend the simulation to a lower temperature region toward $\mathrm{T_{bulk}}$. At this point, it is valuable to reduce the calculation time through acceleration via optimized code tuning that is suitable for the vector parallelization in the SX-Aurora TSUBASA [38].

4 Summary

As described in this paper, a simulation based on the Ginzburg–Landau equation demonstrated the field-induced chiral phenomena due to paramagnetic coupling of an intrinsic magnetization with an external magnetic field in inhomogeneous superconductivity, such as that in a eutectic system and systems with dislocation or

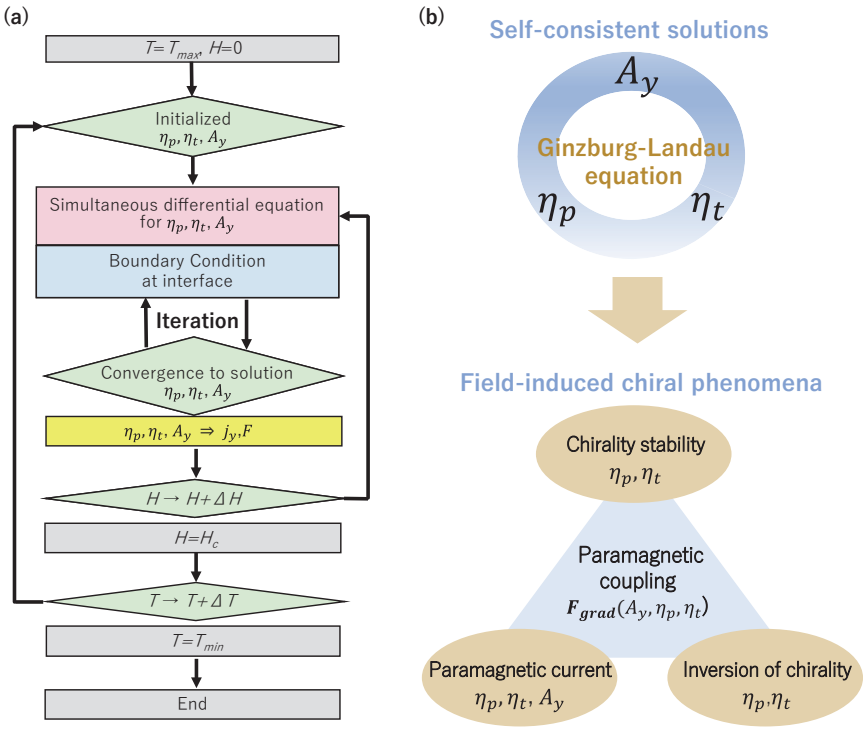

Fig. 6: (a) Field-induced chiral phenomena are the chiral stability, paramagnetic chiral current, and inversion of chirality, accompanied by the gain in the free energy owing to paramagnetic coupling. The simulation based on the Ginzburg–Landau theory shows the relation between the three field-induced phenomena, owing to the chiral response to an external magnetic field. (b) Flowchart of numerical calculation based on the quasi-Newton method.

stress. The simulation demonstrates these phenomena in the interface superconducting model of eutectic Sr_2RuO_4-Ru, and the results of the field-induced chiral transition serve as evidence of the chiral state in the bulk state owing to their good agreement with the experimental results. Using a high-performance computer, the SX-Aurora TSUBASA, for the simulation, the calculation time was reduced through acceleration via code optimization that is suitable for vector parallelization. This reduction of calculation time makes it possible to extend the simulation to a lower-temperature region, which requires the evaluation to be performed considering a longer distance. In addition to Sr_2RuO_4 [19, 21], the simulation can be extended to analyze the inhomogeneous state in other chiral superconductors; field-induced chiral phenomena can also be expected in the inhomogeneous state in other candidates of chiral superconductors, such as UTe_2 with a point group D_{2h} for a crystal structure [8, 27].

Acknowledgements H.K. is grateful to M. Sigrist for the valuable suggestions regarding the theoretical aspects on this work, and acknowledges A. Ramires and Y. Fukaya for the valuable discussions on superconducting states. This work was performed using SQUID at the Cybermedia Center, Osaka University. Further, it was partly performed on the supercomputer SX-ACE at the Cybermedia Center, Osaka University, and Tohoku University. In addition, this study was supported by the Joint Usage and Research of JHPCN (No. jh200032). For the comparison, the performance of the code was evaluated on the supercomputer FUGAKU through the Startup Preparation Project (No. hp200216) of HPCI. This work is also supported by the JSPS Core-to-Core Program No. JPJSCCA20170002.

References

1. J. Bardeen, L.N. Cooper and J.R. Schrieffer. Theory of Superconductivity. *Phys. Rev.* **108**, 1175 (1957). DOI 10.1103/PhysRev.108.1175. URL https://link.aps.org/doi/10.1103/PhysRev.108.1175
2. R. Egawa, K. Komatsu, S. Momose, Y. Isobe, A. Musa, H. Takizawa and H. Kobayashi. Potential of a modern vector supercomputer for practical applications: performance evaluation of SX-ACE. *The Journal of Supercomputing* **73**(9), 3948 (2017). DOI 10.1007/s11227-017-1993-y. URL https://doi.org/10.1007/s11227-017-1993-y
3. S.B. Etter, H. Kaneyasu, M. Ossadnik and M. Sigrist. Limiting mechanism for critical current in topologically frustrated Josephson junctions. *Phys. Rev. B* **90**, 024515 (2014). DOI 10.1103/PhysRevB.90.024515. URL https://link.aps.org/doi/10.1103/PhysRevB.90.024515
4. Y. Fukaya, T. Hashimoto, M. Sato, Y. Tanaka and K. Yada. Spin susceptibility for orbital-singlet Cooper pair in the three-dimensional Sr_2RuO_4 superconductor. *Phys. Rev. Research* **4**, 013135 (2022). DOI 10.1103/PhysRevResearch.4.013135. URL https://link.aps.org/doi/10.1103/PhysRevResearch.4.013135
5. V. Grinenko, D. Das, R. Gupta, B. Zinkl, N. Kikugawa, Y. Maeno, C.W. Hicks, H.H. Klauss, M. Sigrist and R. Khasanov. Unsplit superconducting and time reversal symmetry breaking transitions in Sr2RuO4 under hydrostatic pressure and disorder. *Nature Communications* **12**(1), 3920 (2021). DOI 10.1038/s41467- 021-24176-8. URL https://doi.org/10.1038/s41467-021-24176-8
6. V. Grinenko, S. Ghosh, R. Sarkar, J.C. Orain, A. Nikitin, M. Elender, D. Das, Z. Guguchia, F. Brückner, M.E. Barber, J. Park, N. Kikugawa, D.A. Sokolov, J.S. Bobowski, T. Miyoshi, Y. Maeno, A.P. Mackenzie, H. Luetkens, C.W. Hicks and H.H. Klauss. Split superconducting and time-reversal symmetry-breaking transitions in Sr_2RuO_4 under stress. *Nature Physics* **17**, 748 (2021). DOI 10.1038/s41567-021-01182-7. URL https://doi.org/10.1038/s41567-021-01182-7
7. Y. Imai, K. Wakabayashi and M. Sigrist. Effect of the RuO6 Octahedron Rotation at the Sr2RuO4 Surface on Topological Property. *Journal of the Physical Society of Japan* **83**(12), 124712 (2014). DOI 10.7566/JPSJ.83.124712. URL https://doi.org/10.7566/JPSJ.83.124712
8. L. Jiao, S. Howard, S. Ran, Z. Wang, J.O. Rodriguez, M. Sigrist, Z. Wang, N.P. Butch and V. Madhavan. Chiral superconductivity in heavy-fermion metal UTe_2. *Nature* **579**, 523 (2020). DOI 10.1038/s41586-020-2122-2. URL https://doi.org/10.1038/s41586-020-2122-2
9. H. Kaneyasu, Y. Enokida, T. Nomura, Y. Hasegawa, T. Sakai and M. Sigrist. Properties of the $H-T$ phase diagram of the $3-K$ phase in eutectic Sr_2RuO_4-Ru: Evidence for chiral superconductivity. *Phys. Rev. B* **100**, 214501 (2019). DOI 10.1103/PhysRevB.100.214501. URL https://link.aps.org/doi/10.1103/PhysRevB.100.214501

10. H. Kaneyasu, Y. Enokida, T. Nomura, Y. Hasegawa, T. Sakai and M. Sigrist. Features of Chirality Generated by Paramagnetic Coupling to Magnetic Fields in the 3 K-Phase of Sr_2RuO_4. *JPS Conf. Proc.* **30**, 011039 (2020). DOI 10.7566/JPSCP.30.011039. URL https://journals.jps.jp/doi/10.7566/JPSCP.30.011039
11. H. Kaneyasu, S.B. Etter, T. Sakai and M. Sigrist. Evolution of the filamentary 3-Kelvin phase in Pb – Ru – Sr_2RuO_4 Josephson junctions. *Phys. Rev. B* **92**, 134515 (2015). DOI 10.1103/PhysRevB.92.134515. URL https://link.aps.org/doi/10.1103/PhysRevB.92.134515
12. H. Kaneyasu, N. Hayashi, B. Gut, K. Makoshi and M. Sigrist. Phase Transition in the 3-Kelvin Phase of Eutectic Sr2RuO4–Ru. *Journal of the Physical Society of Japan* **79**, 104705 (2010). DOI 10.1143/JPSJ.79.104705. URL https://doi.org/10.1143/JPSJ.79.104705
13. H. Kaneyasu and M. Sigrist. Nucleation of Vortex State in Ru-Inclusion in Eutectic Ruthenium Oxide Sr2RuO4–Ru. *Journal of the Physical Society of Japan* **79**, 053706 (2010). DOI 10.1143/JPSJ.79.053706. URL https://doi.org/10.1143/JPSJ.79.053706
14. M. Kawamura, H. Yaguchi, N. Kikugawa, Y. Maeno and H. Takayanagi. Tunneling Properties at the Interface between Superconducting Sr2RuO4 and a Ru Microinclusion. *Journal of the Physical Society of Japan* **74**, 531 (2005). DOI 10.1143/JPSJ.74.531. URL https://doi.org/10.1143/JPSJ.74.531
15. S.A. Kivelson, A.C. Yuan, B. Ramshaw and R. Thomale. A proposal for reconciling diverse experiments on the superconducting state in Sr2RuO4. *npj Quantum Materials* **5**(1), 43 (2020). DOI 10.1038/s41535-020-0245-1. URL https://doi.org/10.1038/s41535-020-0245-1
16. K. Komatsu, S. Momose, Y. Isobe, O. Watanabe, A. Musa, M. Yokokawa, T. Aoyama, M. Sato and H. Kobayashi. Performance Evaluation of a Vector Supercomputer SX-Aurora TSUBASA. In: *SC18: International Conference for High Performance Computing, Networking, Storage and Analysis*, pp. 685–696 (2018). DOI 10.1109/SC.2018.00057
17. A.J. Leggett. A theoretical description of the new phases of liquid ^{3}He. *Rev. Mod. Phys.* **47**, 331 (1975). DOI 10.1103/RevModPhys.47.331. URL https://link.aps.org/doi/10.1103/RevModPhys.47.331
18. G.M. Luke, Y. Fudamoto, K.M. Kojima, M.I. Larkin, J. Merrin, B. Nachumi, Y.J. Uemura, Y. Maeno, Z.Q. Mao, Y. Mori, H. Nakamura and M. Sigrist. Time-reversal symmetry-breaking superconductivity in Sr_2RuO_4. *Nature* **394**, 558 (1998). DOI 10.1038/29038. URL https://doi.org/10.1038/29038
19. A.P. Mackenzie, T. Scaffidi, C.W. Hicks and Y. Maeno. Even odder after twenty-three years: the superconducting order parameter puzzle of Sr2RuO4 *npj Quantum Materials* **2**, 40 (2017). DOI 10.1038/s41535-017-0045-4. URL https://doi.org/10.1038/s41535-017-0045-4
20. Y. Maeno, T. Ando, Y. Mori, E. Ohmichi, S. Ikeda, S. NishiZaki and S. Nakatsuji. Enhancement of Superconductivity of Sr_2RuO_4 to 3 K by Embedded Metallic Microdomains. *Phys. Rev. Lett.* **81**, 3765 (1998). DOI 10.1103/PhysRevLett.81.3765. URL https://link.aps.org/doi/10.1103/PhysRevLett.81.3765
21. Y. Maeno, H. Hashimoto, K. Yoshida, S. Nishizaki, T. Fujita, J.G. Bednorz and F. Lichtenberg. Superconductivity in a layered perovskite without copper. *Nature* **372**, 1476 (1994). DOI 10.1038/372532a0. URL https://www.nature.com/articles/372532a0
22. M. Matsumoto, C. Belardinelli and M. Sigrist. Upper Critical Field of the 3 Kelvin Phase in Sr_2RuO_4. *Journal of the Physical Society of Japan* **72**, 1623 (2003). DOI 10.1143/JPSJ.72.1623. URL https://doi.org/10.1143/JPSJ.72.1623
23. M. Matsumoto and M. Sigrist. Quasiparticle States near the Surface and the Domain Wall in a $px \pm ipy$-Wave Superconductor. *Journal of the Physical Society of Japan* **68**, 994 (1999). DOI 10.1143/JPSJ.68.3120. URL https://doi.org/10.1143/JPSJ.68.3120
24. W. Meissner and R. Ochsenfeld. Ein neuer Effekt bei Eintritt der Supraleitf¨ahigkeit. *Naturwissenschaften* **21**, 787 (1933). DOI 10.1007/BF01504252. URL https://doi.org/10.1007/BF01504252
25. H.K. Onnes. Further experiments with liquid helium. D. On the change of electrical resistance of pure metals at very low temperatures, etc. V. The disappearance of the resistance of mercury. *Akad. van Wetenschappen (Amsterdam)* **14**, 113–115 (1911).

26. A. Ramires and M. Sigrist. Superconducting order parameter of Sr_2RuO_4: A microscopic perspective. *Phys. Rev. B* **100**, 104501 (2019). DOI 10.1103/PhysRevB.100.104501. URL https://link.aps.org/doi/10.1103/PhysRevB.100.104501
27. S. Ran, C. Eckberg, Q.P. Ding, Y. Furukawa, T. Metz, S.R. Shanta, I.L. Lin, M. Zic, H. Kim, J. Paglione and N.P. Butch. Nearly ferromagnetic spin-triplet superconductivity. *Science* **365**, 684 (2019). DOI 10.1126/science.aav8645. URL https://www.science.org/doi/abs/10.1126/science.aav8645
28. A.T. Rømer, P.J. Hirschfeld and B.M. Andersen. Superconducting state of Sr_2RuO_4 in the presence of longer-range Coulomb interactions. *Phys. Rev. B* **104**, 064507 (2021). DOI 10.1103/PhysRevB.104.064507. URL https://link.aps.org/doi/10.1103/PhysRevB.104.064507
29. A.T. Rømer, D.D. Scherer, I.M. Eremin, P.J. Hirschfeld and B.M. Andersen. Knight Shift and Leading Superconducting Instability from Spin Fluctuations in Sr_2RuO_4. *Phys. Rev. Lett.* **123**, 247001 (2019). DOI 10.1103/PhysRevLett.123.247001. URL https://link.aps.org/doi/10.1103/PhysRevLett.123.247001
30. T. Shiroka, R. Fittipaldi, M. Cuoco, R. De Renzi, Y. Maeno, R.J. Lycett, S. Ramos, E.M. Forgan, C. Baines, A. Rost, V. Granata and A. Vecchione. μSR studies of superconductivity in eutectically grown mixed ruthenates. *Phys. Rev. B* **85**, 134527 (2012). DOI 10.1103/PhysRevB.85.134527. URL https://link.aps.org/doi/10.1103/PhysRevB.85.134527
31. M. Sigrist and H. Monien. Phenomenological Theory of the 3 Kelvin Phase in Sr_2RuO_4. *Journal of the Physical Society of Japan* **70**, 2409 (2001). DOI 10.1143/JPSJ.70.2409. URL https://doi.org/10.1143/JPSJ.70.2409
32. M. Sigrist and K. Ueda. Phenomenological theory of unconventional superconductivity. *Rev. Mod. Phys.* **63**, 239 (1991). DOI 10.1103/RevModPhys.63.239. URL https://link.aps.org/doi/10.1103/RevModPhys.63.239
33. A. Steppke, L. Zhao, M.E. Barber, T. Scaffidi, F. Jerzembeck, H. Rosner, A.S. Gibbs, Y. Maeno, S.H. Simon, A.P. Mackenzie and C.W. Hicks. Strong peak in T_c of Sr_2RuO_4 under uniaxial pressure. *Science* **355**(6321), eaaf9398 (2017). DOI 10.1126/science.aaf9398. URL https://www.science.org/doi/abs/10.1126/science.aaf9398
34. H.G. Suh, H. Menke, P.M.R. Brydon, C. Timm, A. Ramires and D.F. Agterberg. Stabilizing even-parity chiral superconductivity in Sr_2RuO_4. *Phys. Rev. Research* **2**, 032023 (2020). DOI 10.1103/PhysRevResearch.2.032023. URL https://link.aps.org/doi/10.1103/PhysRevResearch.2.032023
35. J. Xia, Y. Maeno, P.T. Beyersdorf, M.M. Fejer and A. Kapitulnik. High Resolution Polar Kerr Effect Measurements of Sr_2RuO_4: Evidence for Broken Time-Reversal Symmetry in the Superconducting State. *Phys. Rev. Lett.* **97**, 167002 (2006). DOI 10.1103/PhysRevLett.97.167002. URL https://link.aps.org/doi/10.1103/PhysRevLett.97.167002
36. H. Yaguchi, K. Takizawa, M. Kawamura, N. Kikugawa, Y. Maeno, T. Meno, T. Akazaki, K. Semba and H. Takayanagi. Spectroscopy of Sr_2RuO_4/Ru Junctions in Eutectic. *AIP Conference Proceedings* **850**, 543 (2006). DOI 10.1063/1.2354825. URL https://aip.scitation.org/doi/abs/10.1063/1.2354825
37. Y. Ying, N. Staley, Y. Xin, K. Sun, X. Cai, D. Fobes, T.J. Liu, Z.Q. Mao and Y. Liu. Enhanced spin-triplet superconductivity near dislocations in Sr_2Ru_O. *Nat. Com.* **4**, 2596 (2013). DOI 10.1038/ncomms3596. URL https://www.nature.com/articles/ncomms3596
38. S. Yoshida, A. Endo, H. Kaneyasu and S. Date. First Experience of Accelerating a Field-Induced Chiral Transition Simulation Using the SX-Aurora TSUBASA. *Supercomput. Front. and Innov.* **8**, 43 (2021). DOI 10.14529/jsfi210203. URL https://superfri.org/index.php/superfri/article/view/383